nature neuroscience

Volitional modulation of optically recorded calcium signals during neuroprosthetic learning

Kelly B Clancy[1,7], Aaron C Koralek[2,7], Rui M Costa[3], Daniel E Feldman[2,4] & Jose M Carmena[2,5,6]

Brain-machine interfaces are not only promising for neurological applications, but also powerful for investigating neuronal ensemble dynamics during learning. We trained mice to operantly control an auditory cursor using spike-related calcium signals recorded with two-photon imaging in motor and somatosensory cortex. Mice rapidly learned to modulate activity in layer 2/3 neurons, evident both across and within sessions. Learning was accompanied by modifications of firing correlations in spatially localized networks at fine scales.

Brain-machine interfaces (BMIs) have gained great momentum as a therapeutic option for patients with limb loss or immobility[1–4]. In addition, BMI tasks provide a powerful approach for studying sensorimotor learning, as they enable arbitrary mapping between neuronal activity, behavioral output and reward[5]. Recent work used BMI to demonstrate network adaptations in response to output perturbations[6], including specific functional changes in output-relevant neurons[7,8]. However, traditional BMIs based on spatially sparse electrode recordings lack fine-scale spatial information about local networks. To address this issue, we developed a BMI task in awake, head-restrained mice using two-photon calcium imaging to record activity from every neuron in a small field of view (150 × 150 μm). We used this calcium-based BMI procedure (CaBMI) to probe fine-scale network reorganization in cortical layer (L) 2/3 of both primary motor (M1) and somatosensory (S1) cortices during BMI learning.

We trained ten mice expressing the genetically encoded calcium indicator gCaMP6f in L2/3 of M1 or S1 to modulate neural activity in response to auditory feedback (Online Methods, **Supplementary Fig. 1a** and **Supplementary Movies 1** and **2**). This task was adapted from one used previously with electrode-based recordings[9]. Each day, two ensembles containing 1–11 neurons each were chosen to control the task (**Fig. 1a**). The ensembles opposed each other, such that increased activity in one ensemble (E1) above its baseline increased the pitch of the auditory feedback, while increased activity in the other ensemble (E2) decreased the pitch. Reward was delivered when a high-pitched target was reached within 30 s of trial initiation (hit). Incorrect trials (no target within 30 s) were signaled with white noise.

Mice learned the task rapidly (**Fig. 1b**), with initial rapid improvement (1–3 d) followed by slower improvement (4–8 d). Mice performed above chance level after 1 d of training ($N = 10$ mice, $P = 0.0036$ on day 2, $t_8 = 4.07$; **Fig. 1b**). Similar learning occurred using M1 or, more surprisingly, S1 (**Supplementary Fig. 1b,c**). Hit rate increased significantly within each daily session ($N = 72$ sessions, 10 mice, $P = 2.6 \times 10^{-5}$, $t_{43} = 4.7$, $R^2 = 0.34$; **Supplementary Fig. 1d**). Mice reached a criterion performance

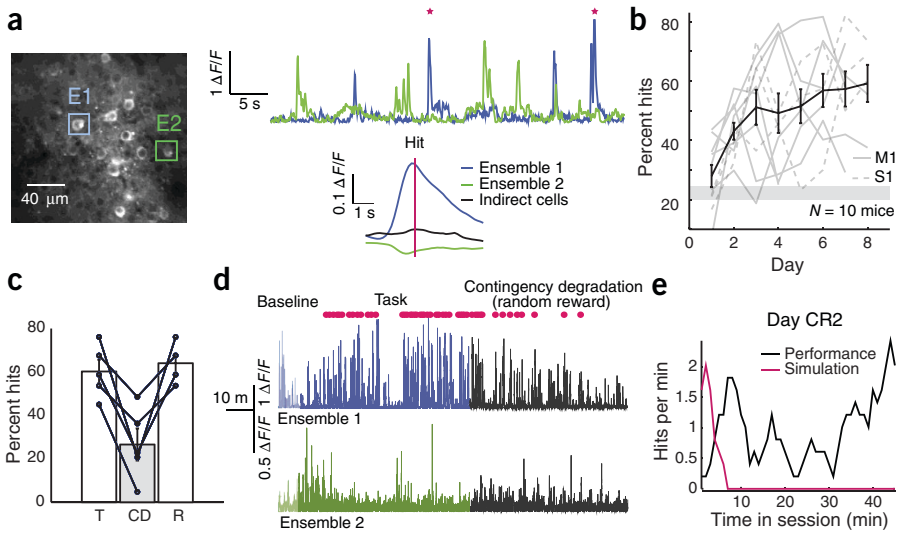

Figure 1 Mice learn to intentionally modulate calcium dynamics. (**a**) Example imaging field (left) and recordings from cells in E1 and E2 (top right). Red stars indicate hits. Bottom right, mean ensemble fluorescence around hits. (**b**) Performance over 8 d of training. Mean performance is shown in black, individual mice in gray. Error bars denote s.e.m. Shaded region denotes chance performance. (**c**) Performance rapidly dropped compared with normal task levels (T) during the contingency degradation (CD). Performance returned to previous levels during reinstatement (R). Error bars represent s.e.m. (**d**) E1 $\Delta F/F$ increased during the task and decreased during CD. Likewise, target hits (red) increased in frequency over training and decreased during CD. (**e**) At the beginning of day CR2, the mouse initially performed as if the previous day's transform algorithm were still in use, but quickly learned the new transform.

[1]Biophysics Program, University of California Berkeley, Berkeley, California, USA. [2]Helen Wills Neuroscience Institute, University of California Berkeley, Berkeley, California, USA. [3]Champalimaud Neuroscience Programme, Champalimaud Center for the Unknown, Lisbon, Portugal. [4]Department of Molecular & Cell Biology, University of California Berkeley, Berkeley, California, USA. [5]Department of Electrical Engineering and Computer Sciences, University of California Berkeley, Berkeley, California, USA. [6]Joint Graduate Group in Bioengineering UCB/UCSF, University of California Berkeley, Berkeley, California, USA. [7]These authors contributed equally to this work. Correspondence should be addressed to R.M.C. (ruicosta@fchampalimaud.org), D.E.F. (dfeldman@berkeley.edu) or J.M.C. (jcarmena@berkeley.edu).

Received 14 February; accepted 2 April; published online 13 April 2014; doi:10.1038/nn.3712

level (50% hits) faster across days of training (N = 8 days, 10 mice, P = 0.0247, t_6 = 2.98, R^2 = 0.596; **Supplementary Fig. 1e**), suggesting that within-session learning occurs faster as between-session learning progresses. As seen previously[9], performance was not impaired by lidocaine injection into the contralateral mystacial pad (N = 4 mice, P = 0.876, t_3 = 0.17) and gross movements were absent preceding target hits, indicating that performance does not rely on natural movement and that neural activity, particularly in S1, is not driven by whisker reafference (**Supplementary Fig. 2**).

We next asked whether these modulations were sensitive to the action-outcome contingency[10]. After mice successfully learned the task, we ceased rewarding target hits and instead delivered rewards under a variable interval schedule (contingency degradation). Mice quickly ceased responding (N = 5 mice, P = 0.0089, t_4 = 4.76; **Fig. 1c,d**). When reward was reinstated using the same E1 and E2 ensembles, mice again performed at normal levels (N = 4 mice, P = 0.791, t_3 = 0.289; **Fig. 1c**). Thus, performance was sensitive to reward contingency, suggesting the behavior is goal directed[11]. *Post hoc* analysis of imaging data revealed that E1 activity increased during task performance and decreased during degradation (**Fig. 1d**). On a separate day, we performed a contingency reversal (N = 3 mice) in which E1 and E2 identities were reversed from one day (day CR1) to the next (day CR2), requiring mice to reverse ensemble activity patterns to obtain reward (**Supplementary Fig. 3a**). Early during CR2, E2 in one example mouse showed clear bursting activity (consistent with its identity as E1 on CR1) and E1 showed little activity (consistent with its identity as E2 on CR1). This pattern quickly reversed as the mouse learned the new contingency (**Supplementary Fig. 3a**). We compared the hit rate on CR2 in one mouse to a simulated hit rate based on the E1/E2 identity and transform algorithm from day CR1. The simulation showed initially high performance that then dropped to zero, indicating that this mouse initially performed according to the learned CR1 transform, but quickly adapted to the new CR2 transform (**Fig. 1e**). Across all mice, the ratio of E1/E2 activity increased during CR2 (**Supplementary Fig. 3b**), suggesting that mice learn to flexibly up-modulate E1 over E2. Together, these data indicate that mice can modulate calcium signals in a contingency-dependent manner and that these modulations can be applied to arbitrarily chosen cells.

We next investigated neural changes during learning. Mean $\Delta F/F$ increased for E1 cells over the course of individual sessions (N = 20 time points, 10 mice, $P = 1.17 \times 10^{-11}$, t_{18} = 15.09, R^2 = 0.927; **Fig. 2a**) and decreased during subsequent contingency degradation (N = 20 time points, 5 mice, P = 0.0029, t_{18} = −3.44; **Supplementary Fig. 4a**). In contrast, mean $\Delta F/F$ did not significantly change for E2 cells (P = 0.234 during task, P = 0.13 during contingency degradation; **Supplementary Fig. 4b,c**). This may reflect a bias toward volitional increases, rather than decreases, of L2/3 calcium dynamics.

Calcium imaging detects activity even in neurons that are rarely active, which are numerous in L2/3 (refs. 12,13). These cells are undersampled by extracellular recordings and are often neglected in BMI studies[14]. There was a 30-fold range of baseline spontaneous activity across L2/3 cells (**Fig. 2b**). We found the most marked increases in task-related activity in E1 cells with initially low baseline (t test of low versus more active E1 cells, N = 72 cells, $P = 8.05 \times 10^{-8}$, t_{70} = 5.99; **Fig. 2b**). Low-baseline E2 cells tended to decrease their activity during task-engagement slightly more than high-baseline cells (t test of low versus more active E2 cells, N = 78 cells, P = 0.02, t_{76} = −2.37; **Fig. 2b**), although mean activity remained unchanged (**Supplementary Fig. 4b**). Thus, task learning preferentially recruited low-active E1 neurons to become more active. These neurons clearly contributed to learning, as learning occurred normally when all E1 cells had low or zero baseline activity (N = 46 sessions, 10 mice, P = 0.83, t_{44} = 1.56; **Supplementary Fig. 5a**), suggesting a role for 'silent' L2/3 neurons in learning[13]. We also found that within multi-cell E1 ensembles, multiple cells increased fluorescence around hits, including low- and zero-baseline cells, indicating that performance was not carried by single neurons (**Supplementary Fig. 5b**).

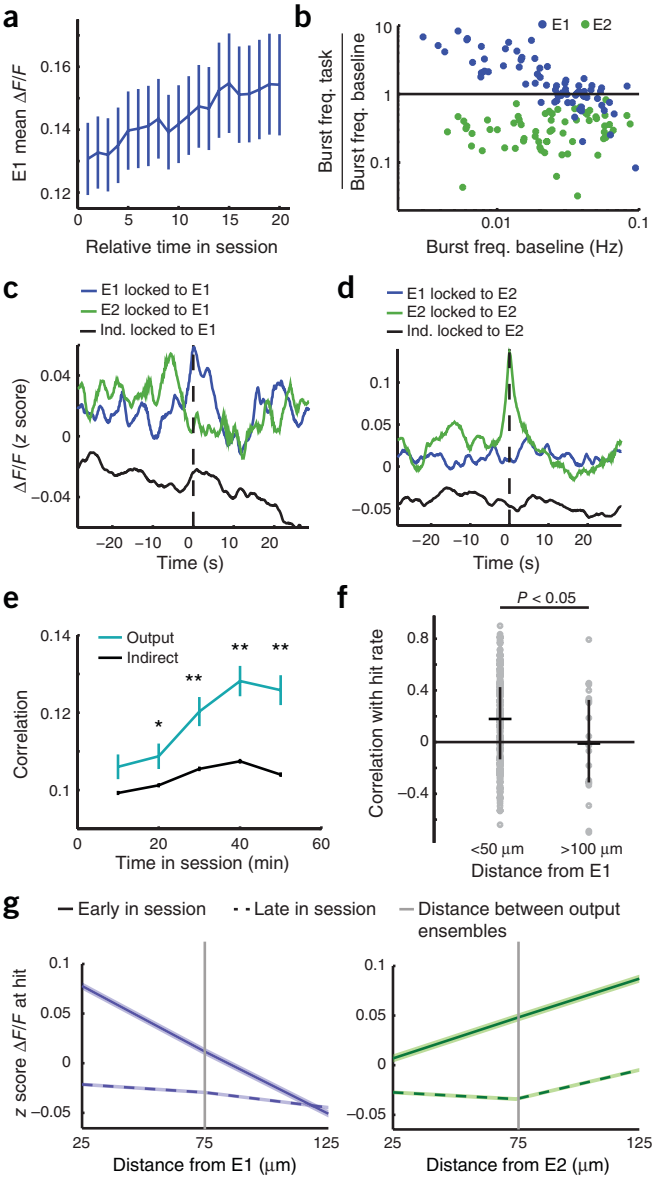

Figure 2 Local network reorganization accompanies neuroprosthetic learning. (**a**) Mean fluorescence increased in E1 cells over the course of a session. Error bars represent s.e.m. (**b**) E1 cells with low baseline activity increased their activity more during the task than cells with high baseline activity. E2 cells suppressed their activity evenly. Note the logarithmic scale. (**c**) Activity in E1, E2 and indirect cells time-locked to large events in E1 cells. (**d**) Activity in E1, E2 and indirect cells time-locked to large events in E2 cells. (**e**) Correlations increased between output cells (cyan) during the session, with no similar increase in correlations between indirect cells (black). $^*P < 0.05$, $^{**}P < 0.001$, Bonferroni corrected. Error bars represent s.e.m. (**f**) Indirect cells near output cells had more task-related activity than those far from output cells. Circles are individual cells, bars indicate s.e.m. Horizontal lines represent the mean. (**g**) Early in a session (solid lines), target-related modulations in indirect cells decreased with distance from E1 cells (blue) and increased with distance from E2 cells (green). Later in the session (dashed lines), there were no significant modulations in indirect cells, regardless of distance from output cells. Shaded areas represent 95% confidence intervals.

To examine higher level network dynamics during learning, we first calculated mean cross-correlation histograms time-locked to the occurrence of large fluorescence events in either E1 or E2 (output cells, Online Methods). Output cells developed coordinated, synchronous activity with other cells in the same ensemble (**Fig. 2c**,**d**). E2 also developed a tendency to spike before E1 (**Fig. 2c**,**d**), likely reflecting a strategy of bursting E2 for trial initiation, followed by bursting of E1 for target achievement. This coordinated activity was not present in non-output cells that were simultaneously imaged (indirect cells; **Fig. 2c**,**d**). This prompted us to investigate correlations between cells over the course of individual sessions. Correlations between output cells in the same ensemble increased significantly during the session ($N = 5$ time points, 10 mice, $P = 0.0198$, $t_3 = 4.55$, $R^2 = 0.874$), whereas correlations between indirect cells did not ($N = 5$ time points, 10 mice, $P = 0.138$, $t_3 = 2.01$; **Fig. 2e**), and this enhancement was observed in individual mice (**Supplementary Fig. 6a**). Output cells also became more correlated over days of training, even though the neural composition of ensembles changed ($N = 8$ d, 10 mice, $P = 0.011$, $t_6 = 3.59$; **Supplementary Fig. 6b**). This is analogous to increased correlations of functionally related cells during motor learning[15] and could reflect millisecond-precision coupling that has been demonstrated with electrodes[16].

We next examined how fine-scale (~10–100 μm) spatial organization of ensembles affects learning. Performance did not vary systematically with distance between output ensembles (measured by E1 and E2 centroids; $N = 71$ sessions, 10 mice, $P = 0.95$, $t_{69} = 0.056$), but did vary with the size of ensembles: mice performed better with fewer neurons, suggesting that it was difficult to maintain coordinated control over large ensembles (**Supplementary Fig. 7**). In addition, high baseline correlations between ensembles predicted worse performance (**Supplementary Fig. 8**).

Learning was accompanied by interesting dynamics in local networks surrounding the output ensembles. For each indirect cell, we calculated the correlation between its mean fluorescence and a moving average of the mouse's instantaneous hit rate. We found that activity in indirect cells near E1 (<50 μm away) was significantly more correlated with hits than activity in distant indirect cells (>100 μm away; $N = 251$ cells, 10 mice, $P = 0.048$, $t_{249} = 1.98$; **Fig. 2f**). Next, we calculated mean target-related modulations in indirect cells for early and late epochs within daily sessions. Early in sessions, indirect cells increased $\Delta F/F$ around hits compared with late in sessions (*t* test early versus late modulations, 437 cells, 5 mice, $P = 3.94\text{e-}4$, $t(436) = 3.57$; **Fig. 2g**). This was evident in cells close to E1 compared to distant cells (*t*-test early versus late modulations in close cells, 172 cells, 5 mice, $P = 0.001$, $t_{171} = 3.32$; *t* test early versus late modulations in distant cells, 265 cells, 5 mice, $P = 0.08$, $t_{264} = 1.72$). Thus, early in the session mice up-modulate activity in a local network surrounding E1 cells[7], but, as the session progresses, this task-related modulation in indirect cells disappears, such that mainly output cells exhibit task-related increases in activity. This suggests that mice are able to hone in on individual output cells during learning and precisely modulate these cells for efficient target achievement[17]. However, even late in sessions, indirect neurons that were more highly spontaneously correlated with E1 cells, and therefore more likely to be embedded in the same local subnetwork[18], exhibited increased activity during task engagement compared with cells with low spontaneous correlations with E1 ($N = 851$ cells, 10 mice, $P = 2.35 \times 10^{-5}$, $t_{849} = 4.26$; **Supplementary Fig. 9a**). Indirect neurons that were more highly spontaneously correlated with E2 cells exhibited decreased activity during task engagement compared with cells with low spontaneous correlations with E2 ($N = 851$ cells, $P = 0.015$, $t_{849} = -2.6$; **Supplementary Fig. 9b**). Given the rapid falloff of spontaneous correlations with distance, such fine-scale effects might be undetectable by electrode-based recording methods (**Supplementary Fig. 9c**). This spatial restriction in activity is similar to sparsening of cortical representations during classical conditioning[19].

To the best of our knowledge, our results represent the first demonstration that mice can volitionally modulate calcium dynamics in L2/3 of M1 and S1, and our use of imaging enabled dissection of learning-related network modifications during BMI with unprecedented spatial resolution (~10–100 μm). Notably, the CaBMI procedure provides a powerful tool for investigating the spatial extent of functional and structural plasticity during neuroprosthetic learning.

METHODS

Methods and any associated references are available in the online version of the paper.

Note: Any Supplementary Information and Source Data files are available in the online version of the paper.

ACKNOWLEDGMENTS

We thank V. Jayaraman, R. Kerr, D. Kim, L. Looger and K. Svoboda for generously sharing gCaMP material, and V. Athalye and K.D. Smith for technical assistance. This work was supported by US National Institutes of Health grant 1R01NS072416-01 to D.E.F., National Science Foundation grant CBET-0954243 to J.M.C., European Research Council grant 243393 to R.M.C. and National Science Foundation Graduate Research Fellowship grant DGE 1106400 to K.B.C.

AUTHOR CONTRIBUTIONS

K.B.C., A.C.K., R.M.C., D.E.F. and J.M.C. designed the experiments. K.B.C. and A.C.K. built the experimental apparatus, performed the experiments and analyzed the data. K.B.C. performed surgical procedures. A.C.K. and K.B.C. wrote the paper. K.B.C., A.C.K., R.M.C., D.E.F. and J.M.C. revised the paper.

COMPETING FINANCIAL INTERESTS

The authors declare no competing financial interests.

1. Nicolelis, M.A.L. *Nature* **409**, 403–407 (2001).
2. Carmena, J.M. *et al. PLoS Biol.* **1**, e42 (2003).
3. Hochberg, L.R. *et al. Nature* **485**, 372–375 (2012).
4. Collinger, J.L. *et al. Lancet* **381**, 557–564 (2013).
5. Green, A.M. & Kalaska, J.F. *Trends Neurosci.* **34**, 61–75 (2011).
6. Jarosiewicz, B. *et al. PNAS* **105**, 19486–19491 (2008).
7. Ganguly, K., Dimitrov, D.F., Wallis, J.D. & Carmena, J.M. *Nat. Neurosci.* **14**, 662–667 (2011).
8. Koralek, A.C., Costa, R.M. & Carmena, J.M. *Neuron* **79**, 865–872 (2013).
9. Koralek, A.C., Jin, X., Long, J.D. II, Costa, R.M. & Carmena, J.M. *Nature* **483**, 331–335 (2012).
10. Hilário, M.R.F., Clouse, E., Yin, H.H. & Costa, R.M. *Front. Integr. Neurosci.* **1**, 6 (2007).
11. Dias-Ferreira, E. *et al. Science* **325**, 621–625 (2009).
12. O'Connor, D.H., Peron, S.P., Huber, D. & Svoboda, K. *Neuron* **67**, 1048–1061 (2010).
13. Barth, A.L. & Poulet, J.F.A. *Trends Neurosci.* **35**, 345–355 (2012).
14. Shoham, S., O'Connor, D.H. & Segev, R. *J. Comp. Physiol. A Neuroethol. Sens. Neural Behav. Physiol.* **192**, 777–784 (2006).
15. Komiyama, T. *et al. Nature* **464**, 1182–1186 (2010).
16. Engelhard, B., Ozeri, N., Israel, Z., Bergman, H. & Vaadia, E. *Neuron* **77**, 361–375 (2013).
17. Costa, R.M. *Curr. Opin. Neurobiol.* **21**, 579–586 (2011).
18. Harris, K.D. & Mrsic-Flogel, T.D. *Nature* **503**, 51–58 (2013).
19. Gdalyahu, A. *et al. Neuron* **75**, 121–132 (2012).

ONLINE METHODS

Mice. All animal procedures were performed in accordance with University of California Berkeley Animal Care and Use Committee regulations. 6 C57BL/6J and 4 CD1 male wild-type mice were used in these experiments, ranging in age from postnatal day 30–45. Mice were housed with a 12-h dark, 12-h light reversed light cycle. All behavioral tests were performed in the same cohort of mice.

Surgery. Mice were anesthetized using 2% isoflurane (vol/vol) and placed in a stereotaxic apparatus. Body temperature was maintained at 37 °C using a feedback-controlled heating pad (FHC, 40-90-8D) and a small incision was made in the scalp. The skull was cleaned and a steel headplate was affixed over M1 (1 mm rostral, 1 mm lateral to Bregma) or S1 (1 mm caudal, 3 mm lateral to Bregma) using Metabond dental cement (Parkell, S380). A 3-mm craniotomy was opened over M1 or S1, and 200 nl of AAV2.9 Syn.GCamp6f.WPRE.SV40 (ref. 20) (University of Pennsylvania Vector Core) was injected 250 μm below the pia using a Nanoliter 2000 injector (World Precision Instruments). The tracer was delivered using a pulled glass pipette (tip diameter = 40–60 μm) at a rate of 40 nl min^{-1}. The pipette was left in the brain for 10 min after completion of the injection to prevent backflow. After the pipette was removed, the brain was covered with silicone oil (Sigma product #181138) and a glass coverslip was affixed to the skull with dental cement, as previously described[21]. We allowed 2 weeks for recovery and gCaMP6f expression.

Two-photon imaging. *In vivo* imaging was performed with a Moveable Objective Microscope (Sutter) using a Chameleon Ultra Ti:Sapphire mode-locked laser (Coherent) tuned to 900 nm. Photons were collected with a Hamamatsu photomultiplier tube (H10770PA-40) using a Nikon objective (16×, 0.8 NA). Animals were head-fixed on a custom-made spring mounted imaging platform and placed under the two-photon microscope. This setup allowed them to run freely, and their movements were recorded by an accelerometer fixed to the underside of the platform. Frames of 128 × 512 pixels (~160 × 160 μm) were collected at 7.23 Hz using ScanImage software[22] at 130–180 μm below the pia. The same imaging fields were used every day, localized by landmarks in the surface blood vessels. Imaged fields were stable over the course of training, and because the cortex was stabilized by a snugly fitting coverslip, only severe movements caused motion artifacts. Motion correction for slow drift in the imaging field was performed manually. Any period of gross movement during the task that caused cells to move out of their regions of interest (ROIs) resulted in poor task performance, as $\Delta F/F$ of E1 was reduced. In this sense, mice were punished for excessive movement and seem to have learned to remain still during the task (**Supplementary Fig. 2c**).

Behavioral task. Two ensembles of 1–11 single cells each were chosen for inclusion in the output population. Cells with bright nuclei, indicating overexpression, were excluded, as were cells with many, poorly separable calcium events, an activity pattern indicative of fast-spiking interneurons. No other selection criteria were used to partition the recorded cells into each ensemble. We also ensured that many cells with good signal were included in the indirect population to enable a proper comparison. The cells assigned to the output population were changed on some days.

Ensemble activity was measured as mean $\Delta F/F$ for all component neurons. Fluorescence values from these ensembles were binned in 200-ms bins and entered into an online transform algorithm that related neural activity to the pitch of an auditory cursor. By modulating activity in these ensembles, rodents controlled the pitch of the cursor. The modulations that we required of the mice were calibrated daily based on a baseline recording session of roughly 2 min. Next, 10–15 min of spontaneous baseline activity was recorded to assess chance levels of performance. Fluorescence values were smoothed by a moving average of the past three time points. Changes in the frequency of the auditory cursor were binned in quarter-octave intervals to match rodent psychophysical discrimination thresholds[23]. Mice then had to modulate calcium dynamics in these neuronal ensembles to move the cursor to a high-pitched target tone that was associated with a 10% sucrose (wt/vol) solution reward. A trial was marked incorrect if a target was not achieved within 30 s of trial initiation. A trial was self-initiated when E1 and E2 activity returned to baseline levels (either by decreased activity in E1 or increased activity in E2), which reset the tone to its starting pitch.

Chance levels of performance (**Fig. 1b** and **Supplementary Fig. 1b**,**c**) were determined by running the animal on the task without reward or auditory feedback. Hits resulted when spontaneous fluctuations were large enough push the decoder to the target frequency. Failure to hit a target in 30 s resulted in a miss. The chance region, plotted in gray in **Figure 1b**, represents the mean chance performance and s.e.m., pooled over all animals and all days.

ROIs were extracted from recorded neural data in real time. These ROIs were entered into custom routines in MATLAB (MathWorks) that translated fluorescence levels into the appropriate feedback pitch and played the pitch on speakers mounted on two sides of the imaging platform. Frequencies used for auditory feedback ranged from 1–24 kHz in quarter-octave increments. When a target was hit, a MATLAB-controlled Data Acquisition board (National Instruments) triggered the operant box to supply the appropriate reward to rodents. Each daily training session lasted 48 ± 2 min (71 ± 4 trials).

Data analysis. All analyses were performed with custom written routines in MATLAB. Recorded movies were spatially aligned using the dftregistration routine in MATLAB[24]. ROIs were manually selected to include the soma of neurons that appeared consistently throughout all recorded movies. Fluorescence traces were extracted from each ROI and data is presented as the relative change in fluorescence, $\Delta F/F$.

No statistical methods were used to pre-determine sample sizes, but our sample sizes are similar to those generally employed in the field. For analyses of behavioral performance during the contingency degradation (**Fig. 1c**), the first ten trials of a session were removed before calculating performance to exclude the transition period and reflect the animal's performance once the animal had fully learned the new reward contingency. For all sliding window analyses, sessions were divided into an equal number of bins to determine the window size, and the step size was a fraction of this window size.

For the data plotted in **Figure 2g**, mean z-score values during task engagement were binned by distance from E1 or E2 centroid. The first bin included all cells from 0–50 μm from the centroid of the output ensemble (close cells), the second bin included all cells 50–100 μm from the output ensemble, and the final bin including all cells 100+ μm from the output ensemble. 'Distant' cells included all cells at a distance of greater than 50 μm from the E1 centroid. We included data from 3 d late in training from 5 mice where 20 or more indirect cells were apparent in the field.

For the cross-correlation histograms, fluorescence traces from output cells were z-scored and values above 3 s.d. were considered an event. The first time point in which fluorescence values crossed this threshold during each event was used for time-locking. Fluorescence values in other populations of cells were then averaged around these indices.

In all cases, multiple comparisons were controlled for using the Bonferroni correction. Differences between groups were tested with t tests. To evaluate trends over time, we tested whether the slope of a fitted linear regression was significantly different from zero. All statistical tests were two-tailed.

For testing the activity modulations for low versus more active cell groups in **Figure 2b**, the high active group included cells with spontaneous event rate greater than the median spontaneous event rate, the low active group included cells with spontaneous event rate less than the median.

Data distributions were assumed to be normal, but this was not formally tested. Data collection and analysis were not performed blind to the experimental conditions. Randomization was not performed, as the experiment primarily involved within-animal comparisons and there were no multiple experimental cohorts. A **Supplementary Methods Checklist** is available.

20. Chen, T.-W. *et al. Nature* **499**, 295–300 (2013).
21. Holtmaat, A. *et al. Cold Spring Harb. Protoc.* **2012**, 694–701 (2012).
22. Pologruto, T.A., Sabatini, B.L. & Svoboda, K. *Biomed. Eng. Online* **2**, 13 (2003).
23. Han, Y.K., Köver, H., Insanally, M.N., Semerdjian, J.H. & Bao, S. *Nat. Neurosci.* **10**, 1191–1197 (2007).
24. Guizar-Sicairos, M., Thurman, S.T. & Fienup, J.R. *Opt. Lett.* **33**, 156–158 (2008).